Effect of Phase Transition and High Pressure on Trace Element Partitioning Between Metal and Sulfide Melt

Robert Thomas

Advisors

Dr. Andrew Campbell
University of Maryland, College Park

Dr. Yingwei Fei
Carnegie Institute Geophysical Laboratory

April 27, 2007

GEOL 394

Abstract

This project examined the effect of the change in the iron crystal structure from fcc to the hcp on the partitioning of rhenium, osmium, platinum and nickel, and whether an increase in pressure of 6 GPa effected the partitioning of those elements. This study was motivated by the Os-isotope work of Brandon et al. and Walker et al. (1995), who interpreted their data in terms of fractional crystallization of the Earth's inner core. In my experiments mixtures of iron, sulfur, nickel and trace amounts of rhenium, osmium and platinum were combined with increasing amounts of ruthenium, to force the crystal structure of iron-ruthenium alloy to change from fcc to hcp. The 1 bar experiments were run in a Deltech furnace and high pressure experiments were run in a multi-anvil press. The samples were analyzed by using both an electron microprobe and a laser ablation ICP-MS to obtain the appropriate partitioning data. The crystal structure change produced an hcp/fcc ratio of 0.26 $\pm$ 0.13 for rhenium and 0.34 $\pm$ 0.15 for platinum, and showed no resolvable effect on osmium. The 6 GPa increase in pressure produced ratios of 0.35 $\pm$ 0.06 for rhenium, 1.67 $\pm$ 0.10 for platinum and 0.44 $\pm$ 0.12 for osmium. Our data suggest that the differences between the partitioning values required by the Brandon et al. (2003) core crystallization models and those observed in the Fe-S system at 1 bar can be reconciled partly by the effects of crystal structure and/or pressure.

Table of Contents

Introduction

The Earth is a differentiated planetary body with a crust, mantle, liquid outer core and a solid metal inner core. The core is mostly iron; according to one model, the major elements (>1 wt %) that make up the core are iron (85.5%), nickel (5.2%), silicon (6%), and sulfur (1.9%) (McDonough, 2003). Accordingly, other highly siderophile elements are also predominantly in the core. The trace elements that are important to this project are rhenium, osmium, and platinum.

It has been proposed, on the basis of osmium isotope measurements of mantle-derived rocks, that material from the core becomes entrained in the overlying mantle flow, and makes its way to the Earth's surface. Radioactive isotopes of both rhenium and platinum decay into isotopes of osmium; these isotopic systems are useful for investigating the evolution of the core because all of the participating elements are highly siderophile, and have very long decay constants. ^{187}Re undergoes decay to yield ^{187}Os, with a half-life of 4.1×10^{10} years. ^{190}Pt undergoes decay to yield ^{186}Os, with a half-life of 4.5×10^{11} years. Walker et al. (1995) and Brandon et al. (1998; 1999; 2003) studied coupled enrichments of ^{186}Os/^{188}Os and ^{187}Os/^{188}Os in mantle derived materials, including modern Hawaiian basalts. The plots of ^{186}Os/^{188}Os vs. ^{187}Os/^{188}Os for the mantle rocks studied did not trend the same as the Primitive Upper Mantle growth line or toward the present-day upper mantle average composition. Instead the plots trended towards a point that would require a mixing between the mantle and a source enriched in platinum, rhenium and osmium. Walker et al. (1995) hypothesized that the ^{186}Os and ^{187}Os-enriched source may have been generated due to crystallization of the solid inner core and consequent increases in Pt/Os and Re/Os in the outer core. If correct, this hypothesis makes several important statements about processes in the deep Earth, including 1) the core and mantle exchange material; and 2) material from the core-mantle boundary can be expressed on the surface of the crust via upwelling plumes.

Walker et al. (1995) and Brandon et al. (1998; 1999; 2003) used some important assumptions to arrive at their conclusions. Some of these can be tested experimentally. Walker and Brandon assumed that rhenium, osmium and platinum partitioning between the solid inner core and liquid outer core of the Earth was similar to the partitioning in iron meteorites. They also assumed that the differences in composition between the Earth's outer core and the melt from which the iron meteorites crystallized were sufficiently small. Finally, they assumed that the effect of pressure on partitioning and the effect of any phase transitions in the metal does not affect the outcome of their model.

This project was designed to test some of the assumptions of the Walker and Brandon hypothesis. Specifically, I examined the effects of pressure change and also change in crystal structure on the partitioning of rhenium, osmium, and platinum between solid metal and sulfide melt.

Iron has three different crystal structures depending on temperature and pressure. Figure 1 is the temperature-pressure phase diagram for iron, showing iron in the body centered cubic (bcc) structure at low temperatures and pressures, the face centered cubic (fcc) structure at higher temperatures and pressures, and the hexagonal close packed (hcp) crystal structure at very high temperatures and pressures. This figure also shows the

pressures at both the core-mantle boundary (CMB) and the inner core-outer core boundary (ICB). The problem with running experiments to recreate core conditions is the need for high pressures in order to obtain the hcp structure of iron. Trace element partitioning experiments at sufficiently high pressures and temperatures to involve hcp-Fe and coexisting melt are not feasible. An alternative way to produce the hcp structure of iron-rich metal at low pressures is to alloy it with ruthenium. Ruthenium has an hcp structure at all temperatures and pressures, and when iron is alloyed with ruthenium, the hcp crystal structure can be obtained regardless of the pressure of the experiment (Fig. 2). This project will utilize Fe-Ru analogs to mimic the high-pressure phase of iron; the effect of ruthenium on the iron crystal structure is to produce the hcp structure of iron at one atmosphere. In addition, the effect of pressure will be investigated using a multi-anvil press to perform metal/melt partitioning experiments involving hcp Fe-Ru alloys, as well as fcc-iron.

Experimental Methods

One Atmosphere Experiments

The one atmosphere experiments were performed by mixing iron, sulfur, ruthenium, nickel, and trace amounts of osmium, rhenium, iridium and platinum in sealed, evacuated silica tubes. It is necessary to perform experiments at a range of Ru contents, to allow the compositional effects of Ru content to be deconvoluted from the effect of the fcc-hcp phase transition. Moreover, it is necessary to perform experiments at a variety of temperatures, to allow the effect of S content of the melt to be understood; metal/melt trace element partitioning is known to be strongly affected by sulfur content in the melt, which varies with temperature according to the phase diagram (Chabot et al., 2003). The mixtures were prepared in eleven different compositions of increasing ruthenium content (Table 1).

The mixtures were weighed by using an electronic scale with 0.00006 g readout precision in the Laboratory for Mineral Deposits Research (LMDR). The compositions were mixed under ethanol with a mortar and pestle; and the samples were then dried in an oven in the Laboratory for Mineral Physics. After the compositions were dried, they were placed in a silica tube that was hooked up to a vacuum source, and sealed with a methane torch (Fig. 3) in the LMDR.

The sealed silica tubes were placed in a Deltech vertical tube furnace in Y. Fei's lab at the Carnegie Institution of Washington. The temperature of the hot spot of the furnace was calibrated using Pt/PtRe thermocouples. The tubes were hung in the hot spot of the furnace by using platinum wire (Fig 4). The temperatures of the experiments were 1300-1500^{o} C in 50^{o} C increments. The tubes remained in the furnace until the solid metal and liquid melt equilibrated. The tubes were then quenched by breaking the platinum wire by running an electrical current through the wire, allowing the tube to fall through the bottom of the furnace into a container of water. After the sample was quenched, it was removed from the silica tube and mounted in epoxy.

High Pressure Experiments

The same compositions used in the one atmosphere experiments were used in the high pressure experiments. All of the high pressure experiments took place in Y. Fei's laboratory at the Carnegie Institution of Washington. The powders were loaded into an 18/11 multi-anvil assembly (Fig 5). The sample holding capsule of the assembly was made of MgO, and the chamber was approximately 1 mm by 0.8 mm. The capsule was placed in a sleeve of MgO, and the sleeve contained the thermocouple on one end and an alumina plug in the other end. The MgO sleeve was then placed in a graphite sleeve, which was the furnace of the assembly. The furnace assembly was then placed in a zirconia sleeve, which was placed in the 18/11 octahedra assembly. The assembly was mounted inside of eight tungsten carbide cubes (Fig 6), and then placed in the multi-anvil apparatus (Fig 7). The sample was then pressurized to 6 GPa. After reaching 6 GPa, the

sample was heated for 24 hours. The temperatures of the experiments were 1100-1500^{o} C in 100^{o} increments. The 6 GPa experiments were run at lower temperatures than the 1 bar experiments, because in this pressure range the melting temperature in the Fe-S system decreases with increasing pressure (Fei et al., 1997). After the heating was finished, the sample was depressurized and removed from the multi-anvil apparatus. The sample was then removed from the octahedra and mounted in epoxy.

Sample Analysis

The mounted sample was polished with wet sandpaper and 1 μm polishing compound until a large area of both the solid metal and quenched sulfide melt was exposed. Microanalysis of the run products was made slightly more difficult by the presence of a dendritic texture that appears in the regions of quenched melt (Figs 8-11). Metal sulfide melts do not quench to a glass. Instead, quenched sulfide melts consist of metal dendrites, surrounded by a matrix of solid sulfide (e.g., Chabot et al., 2003; 2006). Chemical analysis of the quenched melt in the run products must cover a broad enough region of the intergrowth to obtain an accurate composition.

Electron microprobe analyses of the samples took place at the Carnegie Institution of Washington using a JEOL JXA-8900 SuperProbe. The standards used in the microprobe analyses were FeS for iron and sulfur, pure Ru for ruthenium and diopside for nickel. For the analysis, a 10 by 10 grid in the quenched sulfide melt was analyzed in order to obtain 100 data points, each covering a 10 μm x 10 μm area of the sample, and the average weight percent of iron and sulfur in the melt were calculated; this large number of analyses provides suitable coverage over the dendritic intergrowth. Six spots on the solid metal of each sample were analyzed, and the average weight percent of iron and ruthenium in the metal was calculated. A $2\sigma_m$ error was reported for the concentrations, which are expressed in weight percents.

After the samples were analyzed with the electron microprobe, the samples were analyzed by laser ablation ICP-MS in the Plasma Laboratory at the University of Maryland. The laser spots sizes were 35-80 microns, and the laser was scanning across the surface of the sample during analysis; this provided coverage over an area large enough to provide an accurate measurement of the intergrowth in the quenched melt regions, and provided high precision in the metal analyses. Five analyses of the quenched sulfide melt and five analyses of the solid metal were taken for each sample. The standard used for the ICP-MS analysis was Hoba. The isotopes measured were ^{57}Fe, ^{61}Ni, ^{101}Ru, ^{187}Re, ^{190}Os, and ^{195}Pt. These data were used to calculate the partition coefficients of nickel, osmium, rhenium and platinum. First the blank values were subtracted from the average counts for each element to obtain a blank corrected value for each element in each phase. Then the Relative Sensitivity Factor (RSF) for Hoba was calculated by taking the ICP-MS analysis average for each element, dividing that by the ICP-MS analysis average of iron, then dividing that value by the known concentration of the element in Hoba divided by the known concentration of iron in Hoba (Campbell and Humayun, 2005). Next the blank corrected value for each element in each phase was divided by the RSF for that element. The concentration of an element was calculated by taking the RSF corrected value for the element, multiplying that by the concentration of iron in the phase

that was obtained from the electron microprobe, then taking that value and dividing it by the RSF value of iron in the phase. The five measurements were averaged for each element, and $2\sigma_m$ errors are reported. The partition coefficient for the element was calculated by dividing the concentration of the element in the solid phase by the concentration of the element in the melt phase.

Results

The experimental samples were analyzed with an electron microprobe to determine the concentrations of sulfur and iron in the quenched melt phase and of iron and ruthenium in the solid metal phase. The samples were then analyzed with laser ablation ICP-MS to determine the concentrations of nickel, rhenium, osmium and platinum in both the quenched liquid and solid metal phases. The partition coefficients for the samples were calculated by dividing the concentration of the trace element in the solid metal phase by the concentration of the trace element in the quenched melt phase (Table 2):

$$D = \frac{x_{metal}}{x_{melt}} \qquad (1)$$

The errors in the partition coefficients were calculated with the following formula:

$$\sigma_D = \sqrt{D^2\left(\left(\frac{\sigma_{metal}}{x_{metal}}\right)^2 + \left(\frac{\sigma_{melt}}{x_{melt}}\right)^2\right)} \qquad (2)$$

where D is the calculated partition coefficient, X is the concentration of the trace element in the particular phase and σ is the standard error of the mean of the concentration of the trace element in the particular phase. The calculated D values were then plotted against the atomic percent of sulfur in the melt phase (Fig. 12).

The D values were then plotted against the atomic percent of ruthenium in the samples (Fig. 13). Much of the variation seen in Fig. 13 is due to the effect of sulfur. As the sulfur content in the melt increases, the calculated D values increase exponentially (Chabot et al., 2003). Since the partition coefficients for each element are affected by the percentage of sulfur in the melt, the partition coefficients need to be normalized in order to remove the effect of the sulfur on the D values.

Partitioning of siderophile elements between metal and melt in the Fe-S system is well constrained by a large number of data (e.g., Chabot et al. (2003)). Chabot and Jones (2003) fit these data to mathematical equations to parameterize partition coefficients of 13 siderophile elements in the iron-sulfur system. The equation for the parameterized partition coefficients is:

$$D = D_O\left[\frac{1-\chi_S}{1-2\chi_S}\right]^{\beta} \qquad (3)$$

where D_O and β are fitted parameters listed in Table 3 and χ_S is the mole fraction of sulfur in the sample. The plots of the parameterized partition coefficients of nickel, rhenium, osmium and platinum are shown in Figure 14. The experimental data plotted with the Chabot and Jones parameterizations are shown in Figure 15. The experimental data was divided by the parameterized partition coefficients to remove the effect of sulfur on the D values. The errors were calculated by dividing the 2σ values of the experimental D values by the Chabot and Jones parameterizations. The normalized partition coefficients are listed in Table 4.

The normalized partition coefficients were then plotted against the atomic percent of ruthenium in the solid metal phase (Fig 16). The one atmosphere data is color coded according to the crystal structure of iron present in the solid metal phase. The rhenium and platinum data showed a definite effect of the fcc-hcp phase change on the partition coefficients, while the data for osmium showed no resolvable effect of the fcc-hcp phase change on the partitioning.

For the one atmosphere experiments, a least squares fit line was used to determine the normalized partition coefficient both for the fcc metal trend and the hcp metal trend at 31.5 atomic percent ruthenium for rhenium, osmium and platinum. The least-squares fits parameterized the effect of Ru on the partition coefficients within each phase, and the comparison between the fcc and hcp phases was made at 31.5% ruthenium because this composition is near the middle of the phase loop between the two phases. These partition coefficients were then used to find the ratio of the hcp partition coefficient to the fcc partition coefficient to determine the effect of the phase change on the partitioning of rhenium, osmium and platinum. It is assumed that, within the uncertainties of this study, the ratio of partition coefficients for the two solid phases remains constant over different temperatures. The calculated ratios are listed in Table 5. The error in the ratios was calculated by using the following equation:

$$\left(\frac{\sigma_y}{y}\right)^2 = \left(\frac{\sigma_{hcp}}{D_{hcp}}\right)^2 + \left(\frac{\sigma_{fcc}}{D_{fcc}}\right)^2 \qquad (4)$$

where y is the calculated ratio, D is the partition coefficient of the appropriate phase and σ is the error in the partition coefficient of the appropriate phase. For the 6 GPa experiments, a least squares fit line was used to determine the normalized partition coefficients for rhenium, osmium and platinum at 0 atomic percent ruthenium. The ratios of D(hcp-melt)/D(fcc-melt) and the ratios of D(6 GPa)/D(1 bar) presented in Table 5 are the principal results of this study. They indicate the effects of the fcc-to-hcp phase change and the effects of 6 GPa pressure on the partitioning behavior of Re, Os, and Pt between iron-rich metal and sulfide melt.

Discussion

Brandon et al. (2003) developed four models of Earth core crystallization based on their analysis of Os-Re and Os-Pt fractionation in Gorgona Island komatiites. Each of the four different models couple different degrees of Re-Os and Pt-Os fractionation to different crystallization histories of the inner core. The first three models assume crystallization starting at 4.4 Ga, while the fourth assumes crystallization starting at 3.5 Ga. The first model proposes rapid crystallization during the first 100 Ma of inner core growth, until much of the inner core is crystallized. The second model proposes rapid crystallization during the Archean, followed by a slower constant crystallization during the post-Archean. The third model proposes a constant crystallization rate throughout inner core growth. The fourth model proposes rapid crystallization starting at 3.5 Ga throughout the Archean, followed by a constant rate of crystallization during the post-Archean. The parameters used in the four models are listed in Table 6.

An important factor in controlling the fractionation of rhenium, osmium and platinum is the Raleigh Fractionation equation.

$$C_x = C_{Ox}(1-f)^{(D_x-1)} \qquad (5)$$

where C_x is the final concentration of the element, C_{Ox} is the starting concentration of the element, f is the fraction of the original melt left and D_x is the partition coefficient for the element. Dividing the Raleigh Fractionation equations for two elements that fractionate in order to produce a ratio due to the fractionation between the two elements:

$$\frac{C_{\mathrm{Re}}}{C_{Os}} = \frac{C_{O\mathrm{Re}}(1-f)^{(D_{\mathrm{Re}}-1)}}{C_{OOs}(1-f)^{(D_{OS}-1)}} \qquad (6)$$

produces a new equation:

$$\frac{C_{\mathrm{Re}}}{C_{Os}} = \frac{C_{O\mathrm{Re}}}{C_{OOs}}(1-f)^{-(D_{Os}-D_{\mathrm{Re}})} \qquad (7)$$

Equation 7 shows that the important factor in the fractionation of the two elements with regard to core crystallization, besides the ratio of the concentrations of the elements, is the difference in the D values between the two elements.

A plot of D_{Os}-D_{Pt} vs. D_{Os}-D_{Re} for the parameters of the core crystallization models proposed by Brandon et al. (2003) shows the values plotting as a linear trend (Fig. 17). One can infer that the 4 specific models presented by Brandon et al. (2003) (Table 6) are representative of a class of models, lying anywhere along the trend described by those 4 (Fig. 17), that satisfy the Os-isotope constraints of Brandon et al. (2003) equally well. Chabot and Jones (2003) parameterized all available partitioning data for the Fe-S system at 1 bar, with Fe metal in the fcc phase. When the Chabot and Jones curves are plotted on the same graph, it is apparent that the parameters for the Brandon core crystallization models do not fit in the fcc iron trend for D_{Os}-D_{Pt} vs. D_{Os}-D_{Re} (Fig 17). The goal of the experiments conducted for this paper is to find out if increased pressure or an fcc to hcp phase change will reconcile the difference between the Brandon model and the experimental partitioning behavior as described by the Chabot and Jones curve in Figure 17.

Taking the ratios from Table 5 showing the effects of the phase transition on the partitioning of rhenium, osmium and platinum, the Chabot and Jones values of D_{Os}-D_{Pt} and D_{Os}-D_{Re} were recalculated (Table 7) and plotted along with the Brandon parameters (Fig 18). The error on the D_{hcp} curve in Figure 18 is dominated by error on D_{Os}-D_{Re}; the error from the D_{Pt} term was negligible in comparison. The Brandon values do not plot within the corrected Chabot and Jones values in the graph, showing that the parameters that Brandon et al. (2003) used in their proposed models of core crystallization cannot be resolved solely by the effect of phase change on the partitioning of rhenium, osmium and platinum. The effect of the phase change is to move the Chabot and Jones curve in the needed direction, but it overshoots the Brandon et al. (2003) models.

Taking the ratios from Table 5 showing the effects of 6 GPa pressure on the partitioning of rhenium, osmium and platinum, the Chabot and Jones values of D_{Os}-D_{Pt} and D_{Os}-D_{Re} were similarly recalculated (Table 8) and plotted along with the Brandon parameters (Figure 19). The Brandon values fall within the corrected Chabot and Jones values in the graph, suggesting that the elevated pressures found in the Earth's core can make the models proposed by Brandon et al. feasible. The large errors in the graph are due to the large $2\sigma_m$ values in the D values of osmium in the high pressure experiments.

Future studies that could be done to improve the interpretations of this paper could include the investigation of the effect of higher pressures on the partitioning of rhenium, osmium and platinum since the pressure at the inner core/outer core boundary is ~330 GPa (Li and Fei 2003). Pressures of 27 GPa can be generated using the multi-anvil presses used for these experiments. The other light elements that might be included in the make up of the core are silicon, carbon and oxygen (McDonough 2003). The effect of the melt compositions of these elements on the partitioning of rhenium, osmium and platinum should also be investigated. A reduction in the uncertainties on D_{Os}-D_{Re} should be attainable by performing experiments at lower S contents in the melt (i.e., higher temperatures). This is technically challenging in sealed silica tube experiments at 1 bar, but should be achievable at high pressures.

Summary

In order to recreate conditions similar to those in the core of the Earth, iron needs to be studied in the hcp crystal structure. Normally in one atmosphere of pressure and high temperatures, iron is in the fcc crystal structure. One way of forcing iron into the hcp crystal structure is to alloy the iron with ruthenium, an element that favors the hcp crystal structure. By mixing iron, sulfur, nickel, ruthenium and trace elements, the partitioning of the trace elements in conditions similar to those in the core can be observed. The trace elements rhenium, osmium and platinum were chosen for this project due to the decay of radiogenic isotopes of rhenium and platinum into osmium, and the hypothesis by Brandon et al. (2003) that there was a mixing of mantle material and liquid core material that produced elevated osmium fractionation in mantle derived rocks that they studied. Brandon et al. proposed four models of core crystallization based on their studies of $^{186}Os/^{188}Os$ and $^{187}Os/^{188}Os$ coupled enrichments. A plot of D_{Os}-D_{Pt} vs. D_{Os}-D_{Re} for the parameters of the core crystallization models proposed by Brandon et al. do not fit the fcc iron trend for D_{Os}-D_{Pt} vs. D_{Os}-D_{Re} using parameterized 1 bar data from Chabot and Jones (2003). The phase transition of iron and the increased pressure both move the D_{Os}-D_{Pt} vs. D_{Os}-D_{Re} trends of Chabot and Jones in the direction of the Brandon models. The phase transition moves the Chabot and Jones curve too far in the needed direction, and it overshoots the Brandon et al. (2003) models. Within error, the Brandon models fall within the 6 GPa pressure effect on the plot of D_{Os}-D_{Pt} vs. D_{Os}-D_{Re}.

Acknowledgements

I would like to thank the following people for their help and support in this project. First, I would like to thank my advisors, Dr. Andrew Campbell of the University of Maryland and Dr. Yingwei Fei of the Carnegie Institution of Washington. I would also like to thank Yu Wang, Liz Cottrell, and Heather Watson of the Carnegie Institution Geophysical Laboratory High Pressure Group, Bjorn Mysen of the Carnegie Institution Geophysical Laboratory High Temperature Lab, Chris Hadidiacos and David George of the Carnegie Institution Geophysical Laboratory Electron Microprobe, and Bill McDonough and Richard Ash at the University of Maryland College Park ICP-MS. Lastly, I would like to thank my family, my friends, and my professors for all the help and support they have given my throughout this project and throughout my undergraduate career.

Bibliography

Brandon, A., Walker, R., Puchtel, I., Becker, H., Humayun, M. and Revillon, S. (2003) ^{186}Os-^{187}Os systematics of Gorgona Island komatiites; implications for early growth of the inner core. *Earth and Planetary Science Letters*, February 15, 2003, Vol. 206, Issue 3-4, pp.411-426.

Brandon A. D., Walker R. J., Morgan J. W., Norman M. D. and Prichard H. M. (1998) Coupled ^{186}Os and ^{187}Os evidence for core-mantle interaction. *Science*, Vol. 280, pp.1570-1573.

Brandon A. D., Norman M. D., Walker R. J. and Morgan J. W. (1999) ^{186}Os-^{187}Os systematics of Hawaiian picrites *Earth and Planetary Science Letters*, Vol.174, pp.25-42.

Campbell, A. and Humayun, M., (2005) Compositions of group IVB iron meteorites and their parent melt. *Geochimica et Cosmochimica Acta,* Vol. 69 pp. 4733-4744.

Chabot, N., Campbell, A., Jones, J., Humayun, M. and Lauer Jr., (2006) The influence of carbon on trace element partitioning behavior. *Geochimica et Cosmochimica Acta*, Vol. 70, pp.1322–1335.

Chabot, N., Campbell, A., Jones, J., Humayun, M. and Agee, C. (2003) An experimental test of Henry's Law in solid metal-liquid metal systems with implications for iron meteorites. *Meteoritics & Planetary Science*, February 2003, Vol. 38, Issue 2, pp.181-196.

Chabot, N. and Jones, J. (2003) The parameterization of solid metal-liquid metal partitioning of siderophile elements. *Meteoritics & Planetary Science*, October 2003, Vol. 38, Issue 10, pp.1425-1436.

Fei, Y., Bertka, C. and Finger, L. (1997) High-pressure iron-sulfur compound, Fe_3S_2, and melting relations in the Fe-FeS system. *Science*, March 14, 1997, Vol. 275, Issue 5306, pp.1621-1623.

Fei, Y., Li, J., Bertka, C. and Prewitt, C. (2000) Structure type and bulk modulus of Fe_3S, a new iron-sulfur compound. *American Mineralogist*, Vol. 85, pp.1830-1833.

Li, J., Fei, Y., Mao, H., Hirose, K., and Shieh, S. (2001) Sulfur in the Earth's inner core. *Earth and Planetary Science Letters*, December 15, 2001, Vol. 193, Issue 3-4, pp.509-514.

Li, J. and Fei, Y. (2003) Experimental Constraints on Core Composition. *Treatise on Geochemistry, Volume 2,* Elsevier Ltd., pp. 521-546.

McDonough, W., (2003) Compositional model for the Earth's core. *Treatise on Geochemistry, Volume 2,* Elsevier Ltd., pp. 547-566.

Walker, R., Morgan, J. and Horan, M. (1995) Osmium-187 enrichment in some plumes; evidence for core-mantle interaction? *Science,* August 11, 1995, Vol. 269, Issue 5225, pp.819-822.

Appendix A. Tables

Table 1. Experimental Compositions.

Composition number	FeS powder (mg)	Fe powder (mg)	Ru powder (mg)	concentration of Ni (ppm)	concentration each of Re, Os and Pt (ppm)
1	36	76	0	5000	500
2	35	71	6	5000	500
3	33	68	11	5000	500
4	33	64	17	5000	500
5	33	57	22	5000	500
6	32	52	28	5000	500
7	31	47	34	5000	500
8	30	43	39	5000	500
9	29	37	46	5000	500
10	28	31	53	5000	500
11	27	26	59	5000	500

Table 2. Experimental Partition Coefficients.

Sample	tube 6-4	tube 6-1	tube 8-2	tube 6-3	tube 7-7	tube 9-6	tube 8-7	tube 8-5	tube 8-3	tube 8-4	tube 10-6	tube 9-5	tube 8-8	tube 7-8
melt at% S	35.0	36.9	38.6	39.9	44.6	43.6	42.8	42.0	37.1	40.5	40.5	38.3	43.07	42.9
metal at% Ru	3.4	0.0	3.9	6.9	25.2	20.3	24.1	16.3	8.4	12.3	21.6	17.4	31.16	30.0
metal phase	fcc	fcc	fcc	fcc	fcc	fcc	fcc	fcc	fcc	fcc	fcc	fcc	fcc+hcp	fcc+hcp
D(Ni)	1.2	1.3	1.3	1.2	0.9	0.9	0.7	1.0	1.0	1.1	0.9	0.8	0.6	0.6
err D (2σ)	0.04	0.04	0.03	0.1	0.1	0.1	0.05	0.02	0.02	0.04	0.04	0.03	0.04	0.02
D(Re)	48.8	101.2	219.7	776.2	19666.9	4538.7	138.4	2638.4	114.0	780.3	2676.8	900.3	376.5	9404.1
err D (2σ)	9.2	22.6	36.0	291.1	3105.9	3261.1	68.3	1111.9	19.5	313.4	660.1	282.8	311.3	4417.0
D(Os)	54.5	110.1	249.0	915.2	16452.3	3956.5	11315.5	1967.1	93.8	552.2	3495.1	651.2	300.2	6866.6
err D (2σ)	10.5	25.2	42.9	339.3	4394.6	3066.6	6717.1	655.1	16.8	266.1	1767.2	186.7	276.2	3857.2
D(Pt)	14.2	29.3	36.4	68.7	404.5	236.3	790.5	134.5	18.6	59.0	138.0	45.7	202.4	119.0
err D (2σ)	2.3	6.1	4.8	18.5	124.4	213.3	459.7	47.0	2.5	20.6	48.3	9.2	116.2	7.9

Sample	tube 12-8	tube 1-9	tube 1-10	tube 2-10	tube 1-11	tube 2-9	tube 6-9	tube 5-9	pt2-1100	pt3-1200	pt5-1200	pt4-1200	pt1-1100	pt4-1100
melt at% S	43.8	44.1	44.2	45.2	43.5	43.9	43.5	44.2	35.0	28.8	32.8	33.3	33.8	35.9
metal at% Ru	33.9	37.9	46.4	46.2	54.8	38.1	38.6	38.1	4.8	11.1	18.3	15.0	0.0	16.0
metal phase	fcc+hcp	hcp	hcp	hcp	hcp	hcp	hcp	hcp	fcc	fcc	fcc	fcc	fcc	fcc
D(Ni)	0.6	0.5	0.4	0.4	0.5	0.5	0.5	0.6	0.8	0.7	0.6	0.6	0.9	0.5
err D (2σ)	0.1	0.02	0.02	0.02	0.03	0.04	0.1	0.1	0.02	0.01	0.01	0.02	0.04	0.01
D(Re)	3651.1	2082.8	1772.0	1345.1	3779.8	2685.2	6697.8	19375.0	39.8	16.4	29.3	37.3	21.7	82.0
err D (2σ)	2006.0	967.3	1185.3	671.4	3262.1	2410.7	3994.5	13277.6	6.3	4.5	1.9	11.3	5.4	22.4
D(Os)	16523.6	3058.6	5905.7	1853.6	33338.9	12430.2	6133.4	8879.4	48.1	15.0	24.6	37.2	28.5	70.2
err D (2σ)	14734.9	1837.6	775.0	846.7	11495.1	5559.2	3812.4	1620.3	17.4	5.8	1.4	12.7	10.8	20.2
D(Pt)	44.1	41.6	206.8	83.6	324.0	109.9		3134.0	23.4	7.7	10.5	11.6	19.9	25.1
err D (2σ)	22.6	18.7	57.1	29.7	170.0	78.7	2290.9	1787.5	3.1	0.5	0.5	1.5	3.0	2.4

Table 3. Chabot and Jones Equation Parameters.

	Ni	Re	Os	Pt
Do	0.86	2	2	0.81
β	0.6	5	5.1	4.4

Table 4. Normalized Partition Coefficients

Sample	atm% S	atm% Ru	Xs	D(CJ) Ni	Exp D Ni	D/D(CJ)	2σ	D(CJ) Re	Exp D Re	D/D(CJ)	2σ	D(CJ) Os	Exp D Os	D/D(CJ)	2σ	D(CJ) Pt	Exp D Pt	D/D(CJ)	2σ
Tube 6-4	35.02	3.41	0.35	1.37	1.16	0.85	0.03	96.08	48.85	0.51	0.10	103.82	54.51	0.53	0.10	24.45	14.25	0.58	0.10
tube 6-1	36.88	0.00	0.37	1.46	1.35	0.93	0.02	161.13	101.15	0.63	0.14	175.92	110.09	0.63	0.14	38.54	29.27	0.76	0.16
tube 8-2	38.57	3.93	0.39	1.56	1.30	0.84	0.02	280.39	219.74	0.78	0.13	309.53	249.04	0.80	0.14	62.75	36.45	0.58	0.08
tube 6-3	39.85	6.93	0.40	1.65	1.23	0.75	0.04	457.61	776.17	1.70	0.64	510.13	915.19	1.79	0.67	96.56	68.71	0.71	0.19
tube 7-5	42.14	13.92	0.42	1.88	1.05	0.56	0.00	1353.96	3798.18	2.81	0.00	1542.47	3517.51	2.28	0.00	250.84	272.18	1.09	0.00
tube 7-7	44.56	25.16	0.45	2.28	0.89	0.39	0.04	6876.28	19666.87	2.86	0.45	8092.45	16452.31	2.03	0.54	1048.21	404.54	0.39	0.12
tube 9-6	43.58	20.28	0.44	2.09	0.90	0.43	0.02	3272.76	4538.72	1.39	1.00	3794.83	3956.48	1.04	0.81	545.39	236.32	0.43	0.39
tube 8-5	42.00	16.30	0.42	1.86	0.96	0.52	0.01	1253.23	2638.43	2.11	0.89	1425.52	1967.12	1.38	0.46	234.34	134.53	0.57	0.20
tube 8-3	37.10	8.36	0.37	1.47	1.01	0.69	0.01	172.25	114.03	0.66	0.11	188.31	93.80	0.50	0.09	40.87	18.61	0.46	0.06
tube 8-4	40.50	12.31	0.40	1.71	1.07	0.63	0.02	601.42	780.27	1.30	0.52	674.12	552.25	0.82	0.39	122.82	59.03	0.48	0.17
tube 10-6	40.46	21.64	0.40	1.70	0.87	0.51	0.02	592.24	2676.77	4.52	1.11	663.63	3495.11	5.27	2.66	121.16	138.04	1.14	0.40
tube 9-5	38.29	17.35	0.38	1.54	0.82	0.53	0.02	254.00	900.30	3.54	1.11	279.84	651.18	2.33	0.67	57.52	45.73	0.79	0.16
tube 7-8	42.87	29.97	0.43	1.98	0.63	0.32	0.01	2065.52	9404.07	4.55	2.14	2373.06	6866.59	2.89	1.63	363.75	119.04	0.33	0.02
tube 12-8	43.76	33.87	0.44	2.12	0.55	0.26	0.03	3711.78	3651.06	0.98	0.54	4314.73	16523.64	3.83	3.42	609.27	44.13	0.07	0.04
tube 1-9	44.13	37.88	0.44	2.19	0.49	0.22	0.01	4885.74	2082.82	0.43	0.20	5710.69	3058.58	0.54	0.32	775.96	41.63	0.05	0.02
tube 1-10	44.21	46.37	0.44	2.21	0.41	0.18	0.01	5174.04	1772.03	0.34	0.23	6054.61	5905.70	0.98	0.13	816.11	206.78	0.25	0.07
tube 2-10	45.17	46.17	0.45	2.44	0.42	0.17	0.01	11765.76	1345.10	0.11	0.06	13996.25	1853.64	0.13	0.06	1681.61	83.55	0.05	0.02
tube 1-11	43.53	54.79	0.44	2.08	0.45	0.22	0.01	3175.04	3779.84	1.19	1.03	3679.29	33338.93	9.06	3.12	531.03	324.00	0.61	0.32
tube 2-9	43.90	38.14	0.44	2.15	0.48	0.22	0.02	4125.08	2685.24	0.65	0.58	4805.30	12430.15	2.59	1.16	668.59	109.86	0.16	0.12
tube 6-9	43.52	38.61	0.44	2.08	0.52	0.25	0.03	3148.70	6697.77	2.13	1.27	3648.16	6133.38	1.68	1.05				
pr2-1100	34.98	4.78	0.35	1.37	0.81	0.59	0.01	94.97	39.76	0.42	0.07	102.60	48.12	0.47	0.17	24.20	23.42	0.97	0.13
pr3-1200	28.75	11.15	0.29	1.17	0.68	0.58	0.01	26.49	16.39	0.62	0.17	27.90	15.00	0.54	0.21	7.87	7.68	0.98	0.07
pr5-1200	32.80	18.25	0.33	1.29	0.56	0.44	0.01	56.93	29.30	0.51	0.03	60.87	24.61	0.40	0.024	15.43	10.47	0.68	0.03
pr4-1200	33.34	15.02	0.33	1.30	0.61	0.47	0.01	64.03	37.26	0.58	0.18	68.63	37.15	0.54	0.185	17.11	11.56	0.68	0.09
pr1-1100	33.85	0.01	0.34	1.32	0.85	0.65	0.03	72.05	21.69	0.30	0.08	77.40	28.54	0.37	0.140	18.98	19.94	1.05	0.16
pr4-1100	35.88	16.04	0.36	1.41	0.53	0.38	0.01	120.70	81.99	0.68	0.19	131.01	70.17	0.54	0.155	29.89	25.13	0.84	0.08

Table 5. The Experimentally Calculated Ratios.

	Re	Os	Pt
Phase Tranistion	0.257	unresolvable	0.340
error	0.13	N/A	0.15
6 Gpa	0.345	0.435	1.67
error	0.06	0.12	0.10

Table 6. Parameters for Core Crystallization Models Proposed by Brandon.

	Model 1	Model 2	Model 3	Model 4
D(Pt)	2.9	2.9	2.9	2.9
D(Re)	18.25	22.7	26.2	24.1
D(Os)	28.2	36.4	44.2	40.4

Table 7. D(Os)-D(Re) vs. D(Os)-D(Pt) Values with Effect of Phase Transition.

	Re				Os	Pt					
		hcp/fcc ratio	hcp/fcc ratio + σ	hcp/fcc ratio - σ			hcp/fcc ratio				
		0.257	0.125	0.389			0.340				
mol% S	C&J fit	D(Re)	D(Re)	D(Re)	C&J fit	C&J fit	D(Pt)	D Os - D Pt	D Os - D Re	D Os - D Re - σ	D Os - D Re + σ
0	2	0.51	0.25	0.78	2.00	0.81	0.28	1.72	1.49	1.22	1.75
2	2.22	0.57	0.28	0.86	2.22	0.89	0.30	1.92	1.65	1.36	1.94
4	2.47	0.64	0.31	0.96	2.48	0.98	0.33	2.15	1.85	1.52	2.17
6	2.78	0.72	0.35	1.08	2.80	1.08	0.37	2.43	2.08	1.72	2.45
8	3.15	0.81	0.39	1.23	3.18	1.21	0.41	2.77	2.37	1.95	2.79
10	3.60	0.93	0.45	1.40	3.65	1.36	0.46	3.18	2.72	2.24	3.20
12	4.16	1.07	0.52	1.62	4.22	1.54	0.53	3.70	3.15	2.61	3.70
14	4.86	1.25	0.61	1.89	4.95	1.77	0.60	4.35	3.70	3.06	4.34
16	5.75	1.48	0.72	2.24	5.88	2.05	0.70	5.18	4.40	3.64	5.16
18	6.91	1.78	0.86	2.69	7.08	2.41	0.82	6.26	5.30	4.39	6.21
20	8.43	2.17	1.06	3.28	8.67	2.87	0.98	7.70	6.51	5.40	7.62
22	10.48	2.70	1.31	4.08	10.84	3.48	1.18	9.65	8.14	6.76	9.52
24	13.34	3.43	1.67	5.19	13.85	4.30	1.46	12.39	10.42	8.67	12.18
26	17.42	4.48	2.18	6.77	18.19	5.44	1.85	16.34	13.71	11.41	16.01
28	23.47	6.03	2.94	9.13	24.65	7.07	2.41	22.24	18.62	15.52	21.71
30	32.83	8.44	4.11	12.77	34.72	9.50	3.23	31.48	26.28	21.95	30.60
32	48.09	12.36	6.02	18.70	51.25	13.30	4.52	46.73	38.88	32.54	45.23
34	74.64	19.19	9.35	29.03	80.25	19.58	6.66	73.59	61.06	51.22	70.90
36	124.78	32.08	15.63	48.53	135.53	30.77	10.47	125.07	103.45	87.00	119.90
38	230.11	59.16	28.82	89.50	253.02	52.73	17.93	235.08	193.86	163.52	224.20
40	486.00	124.95	60.87	189.03	542.44	101.82	34.62	507.81	417.48	353.41	481.56
42	1251.90	321.86	156.80	486.93	1423.97	234.12	79.62	1344.35	1102.11	937.04	1267.17
44	4426.53	1138.07	554.43	1721.70	5163.74	711.40	241.92	4921.82	4025.68	3442.04	4609.31
46	28025.21	7205.31	3510.22	10900.40	33921.83	3609.29	1227.40	32694.43	26716.52	23021.43	30411.61

Table 8. D(Os)-D(Re) vs D(Os)-D(Pt) Values with Effect of 6GPa Pressure.

	Re		Os		Pt						
		6 Gpa ratio 0.345		6 Gpa ratio 0.435		6 Gpa ratio 1.169					
mol% S	C&J fit	D(Re)	C&J fit	D(Os)	C&J fit	D(Pt)	D(Os)-D(Pt)	D(Os)-D(Re)	σ(Os-Re)	D(Os)-D(Re) + σ	D(Os)-D(Re) - σ
0	2.00	0.69	2.00	0.87	0.81	0.95	-0.08	0.18	0.26	0.44	-0.08
2	2.22	0.76	2.22	0.97	0.89	1.04	-0.07	0.20	0.29	0.49	-0.08
4	2.47	0.85	2.48	1.08	0.98	1.14	-0.06	0.23	0.32	0.55	-0.09
6	2.78	0.96	2.80	1.22	1.08	1.27	-0.05	0.26	0.36	0.62	-0.10
8	3.15	1.09	3.18	1.38	1.21	1.41	-0.03	0.30	0.41	0.71	-0.11
10	3.60	1.24	3.65	1.59	1.36	1.59	0.00	0.34	0.47	0.81	-0.13
12	4.16	1.43	4.22	1.84	1.54	1.80	0.03	0.40	0.54	0.95	-0.14
14	4.86	1.68	4.95	2.15	1.77	2.07	0.08	0.48	0.64	1.11	-0.16
16	5.75	1.98	5.88	2.55	2.05	2.40	0.16	0.57	0.76	1.33	-0.18
18	6.91	2.38	7.08	3.08	2.41	2.82	0.26	0.70	0.91	1.61	-0.21
20	8.43	2.90	8.67	3.77	2.87	3.36	0.42	0.87	1.12	1.98	-0.25
22	10.48	3.61	10.84	4.71	3.48	4.07	0.65	1.10	1.39	2.49	-0.29
24	13.34	4.60	13.85	6.02	4.30	5.03	1.00	1.43	1.78	3.21	-0.35
26	17.42	6.00	18.19	7.91	5.44	6.36	1.55	1.91	2.33	4.24	-0.42
28	23.47	8.08	24.65	10.72	7.07	8.26	2.45	2.63	3.16	5.79	-0.52
30	32.83	11.31	34.72	15.10	9.50	11.10	3.99	3.79	4.44	8.23	-0.66
32	48.09	16.57	51.25	22.28	13.30	15.54	6.74	5.72	6.55	12.26	-0.83
34	74.64	25.72	80.25	34.89	19.58	22.88	12.01	9.18	10.24	19.41	-1.06
36	124.78	42.99	135.53	58.93	30.77	35.96	22.97	15.94	17.26	33.20	-1.31
38	230.11	79.28	253.02	110.02	52.73	61.62	48.40	30.74	32.15	62.89	-1.41
40	486.00	167.45	542.44	235.87	101.82	118.98	116.89	68.42	68.75	137.17	-0.33
42	1251.90	431.33	1423.97	619.19	234.12	273.58	345.60	187.85	179.91	367.77	7.94
44	4426.53	1525.12	5163.74	2245.35	711.40	831.31	1414.04	720.23	649.83	1370.06	70.40
46	28025.21	9655.82	33921.83	14750.24	3609.29	4217.66	10532.57	5094.42	4245.43	9339.85	848.99

Appendix B. Figures

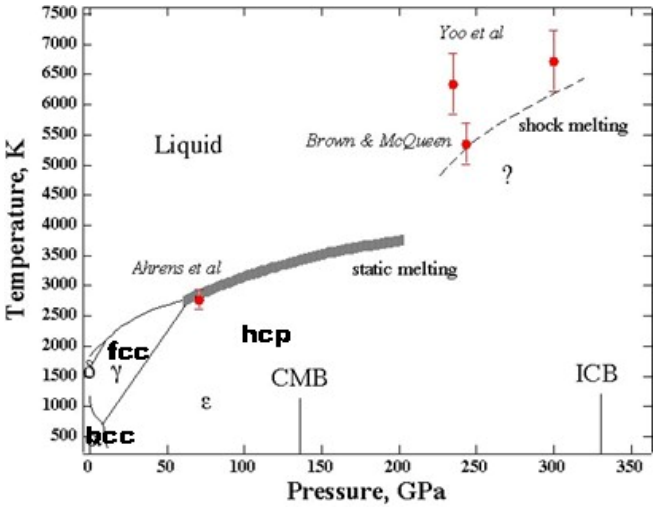

Figure 1. The pressure-temperature phase diagram for iron, showing the three different crystal structures of iron and the pressures at the core-mantle boundary (CMB) and the inner core-outer core boundary (ICB). From Li and Fei (2003).

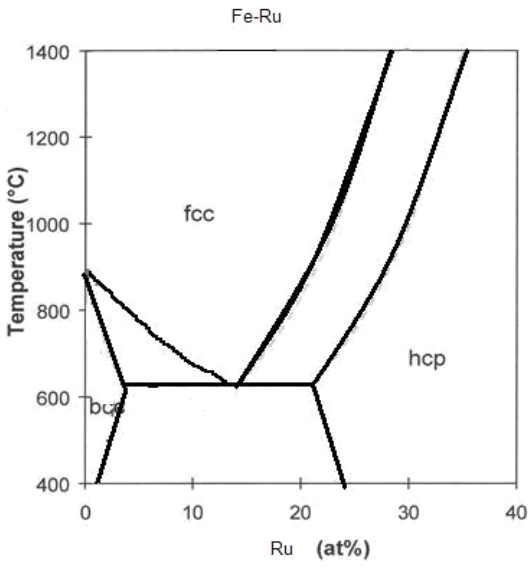

Figure 2. The phase diagram for the iron-ruthenium system showing the temperature and atomic percent of ruthenium needed to change the crystal structure.

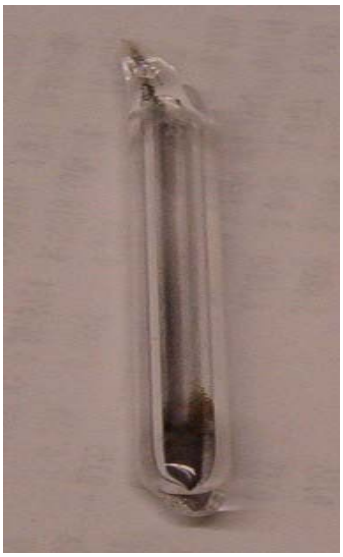

Figure 3. A sealed silica tube with sample powder. This tube was hung in a Deltech vertical furnace until equilibrium was established.

Figure 4. A demonstration of how the silica tubes were hung with platinum wire in the hot spot of the furnace.

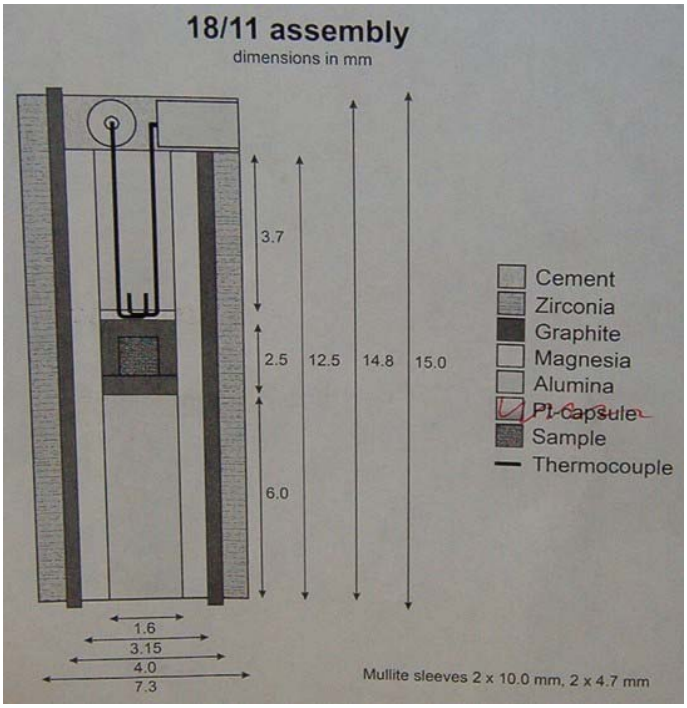

Figure 5. A schematic of the 18/11 multi-anvil assembly that was placed in an 18/11 octahedra and mounted in tungsten carbide cubes.

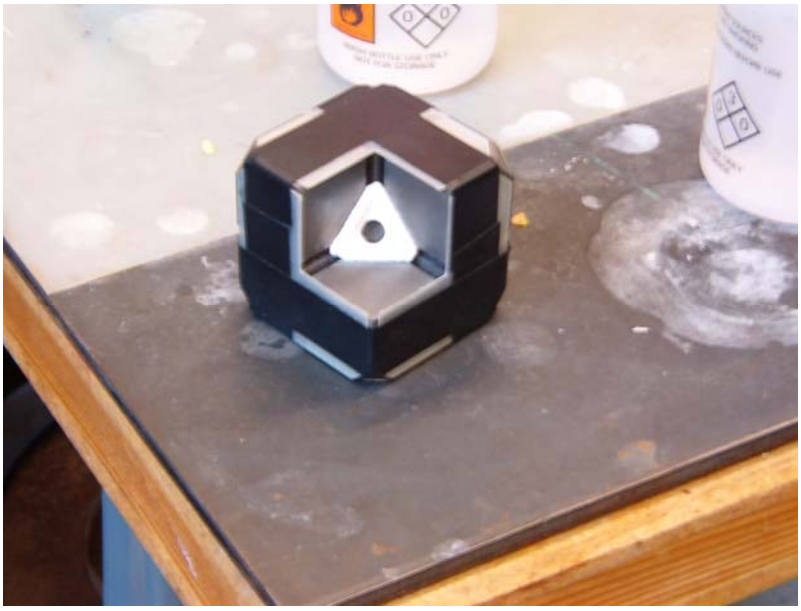

Figure 6. An 18/11 multi-anvil octahedra mounted in tungsten carbide cubes.

Figure 7. The multi-anvil apparatus used for the 6 GPa experiments.

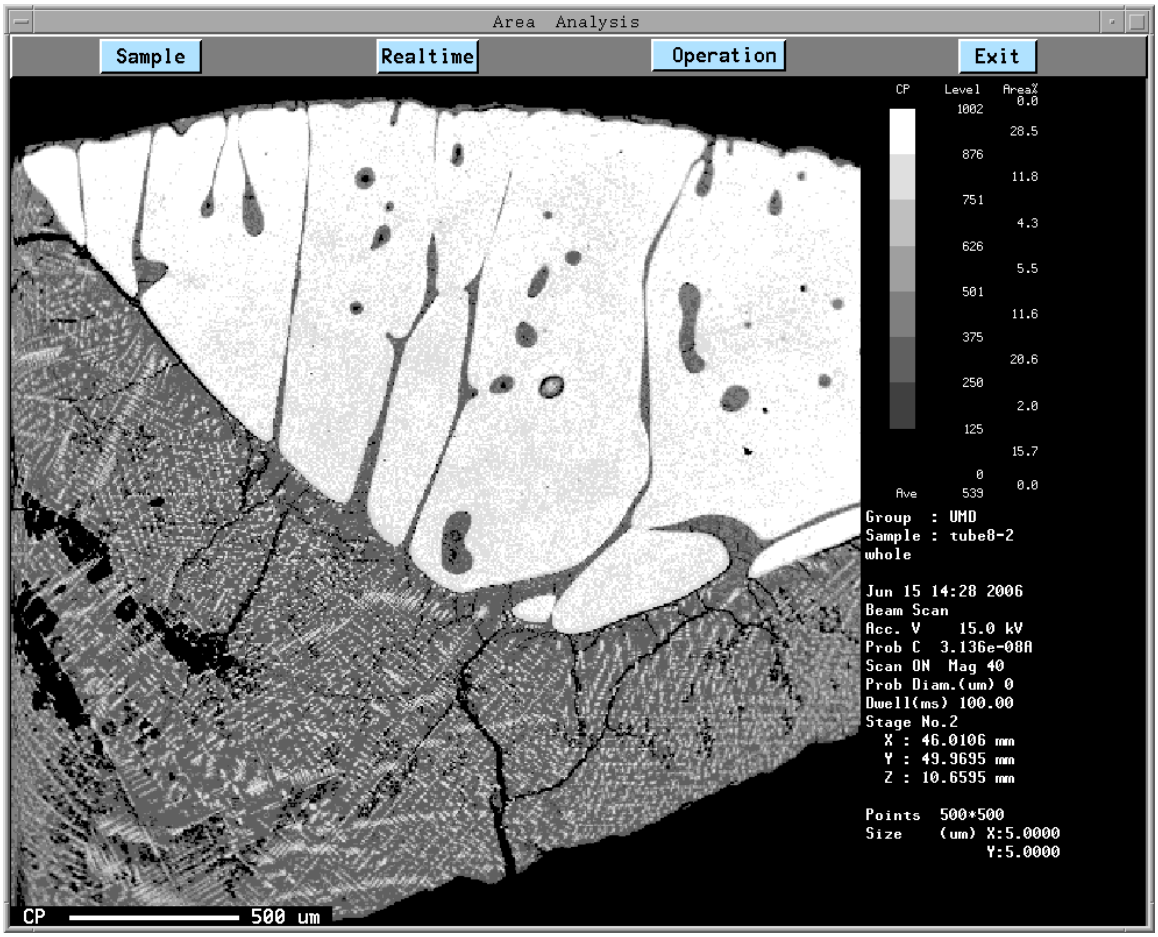

Figure 8. A high resolution back-scattered electron image showing the textures of a quenched one atmosphere experimental sample.

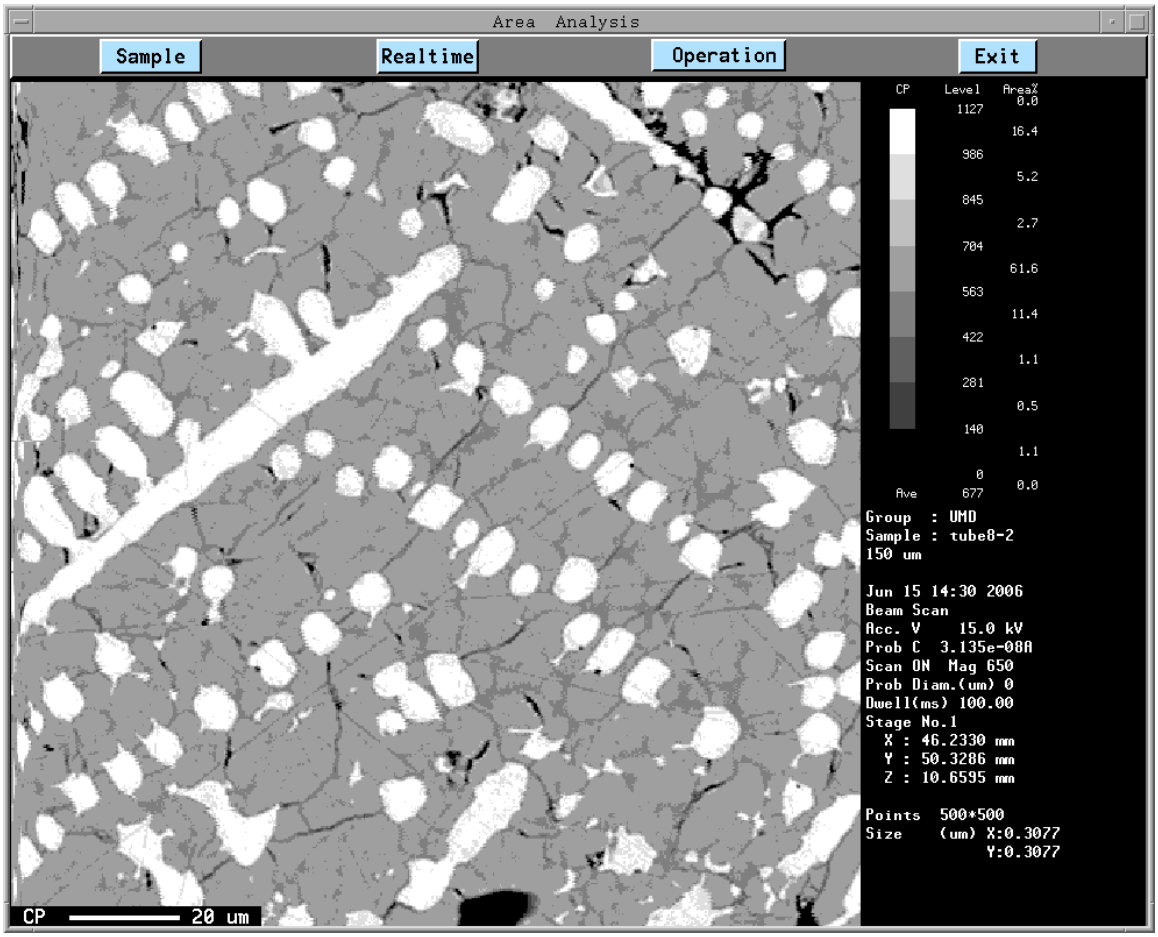

Figure 9. A high resolution back-scattered electron image showing the dendritic quench texture of the sulfide melt in a one atmosphere experimental sample. The area shown in the image is the area that was analyzed to obtain the concentrations of iron, sulfur and ruthenium in the quenched melt.

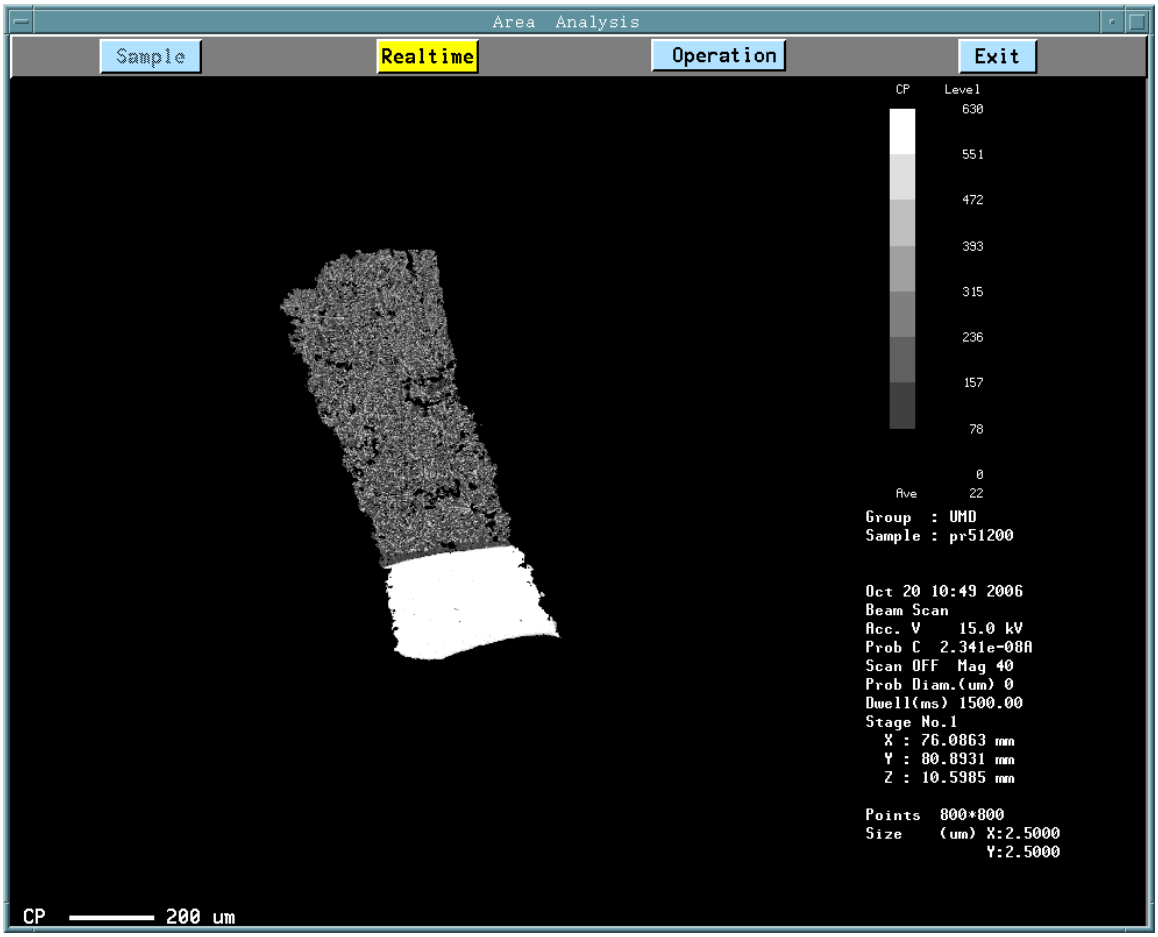

Figure 10. A high resolution back-scattered electron image of a 6 GPa experimental sample.

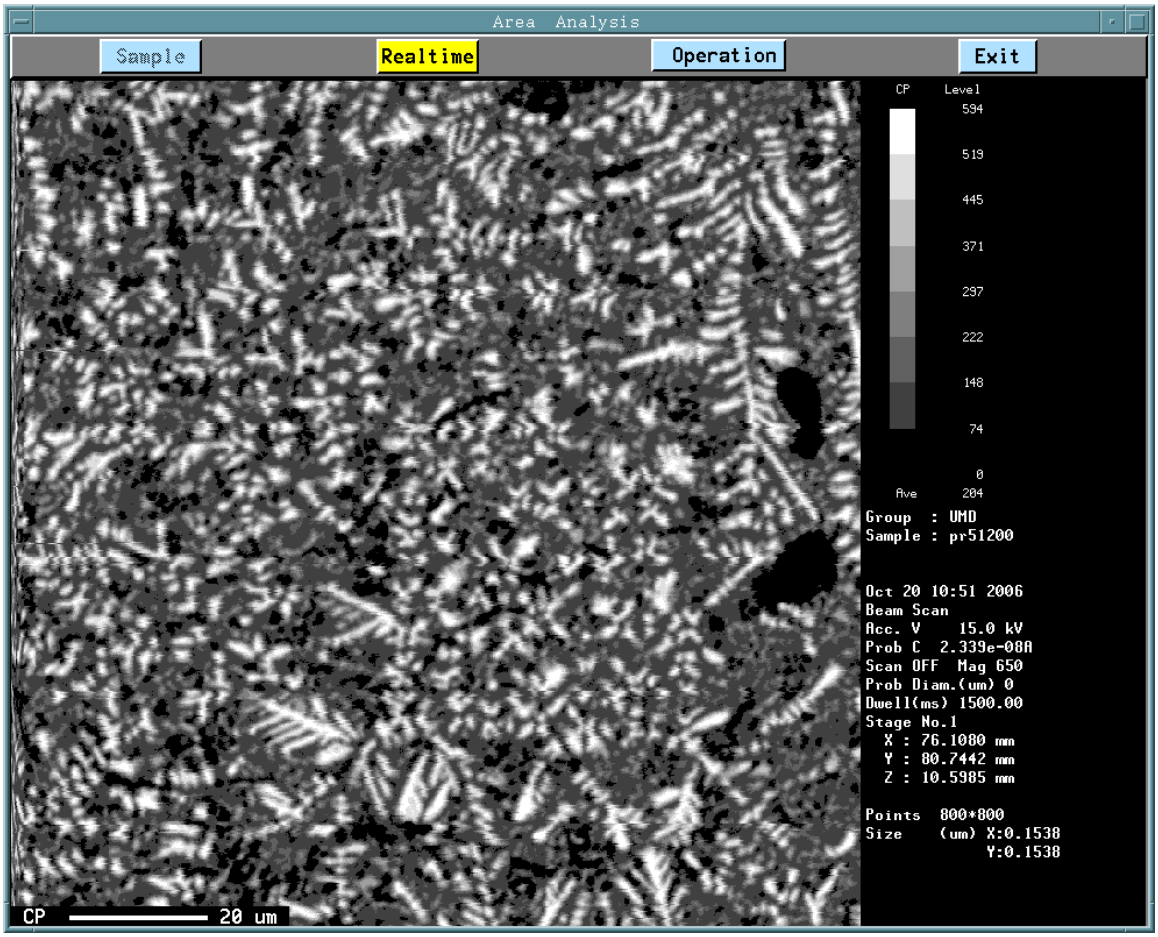

Figure 11. A high resolution back-scattered electron image of the sulfide melt quench texture of a 6 GPa experimental sample.

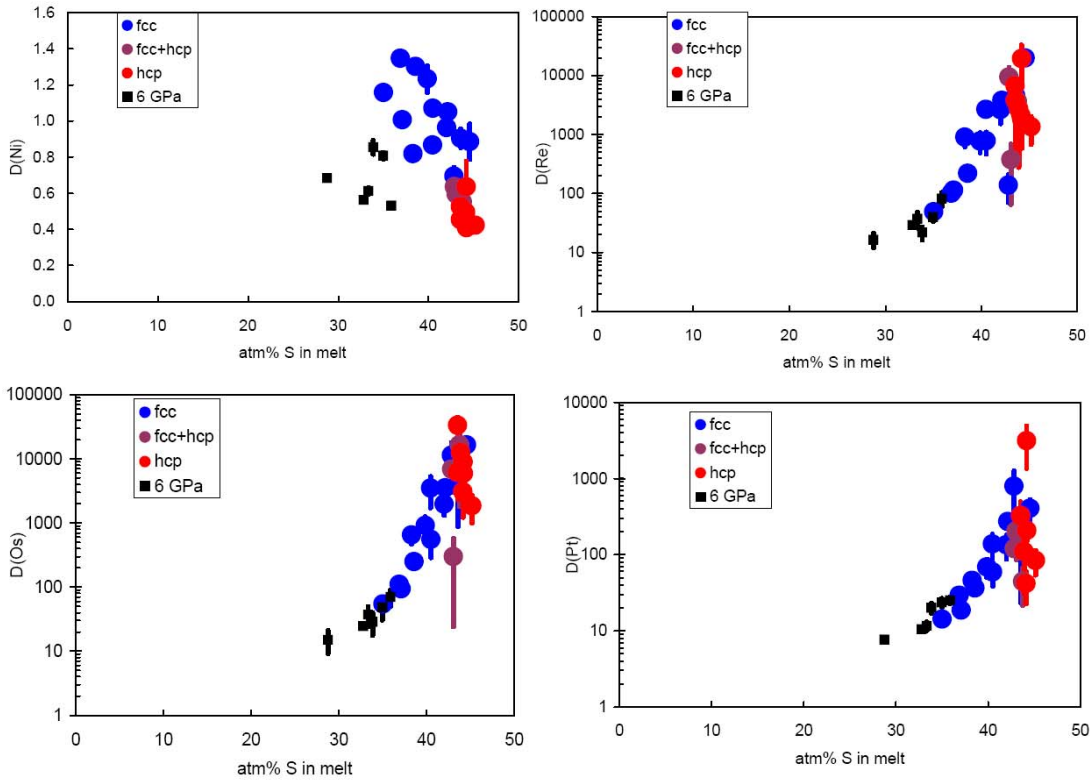

Figure 12. Graphs of the experimental D values of nickel, rhenium, osmium and platinum plotted against the sulfur content in the quenched melt phase.

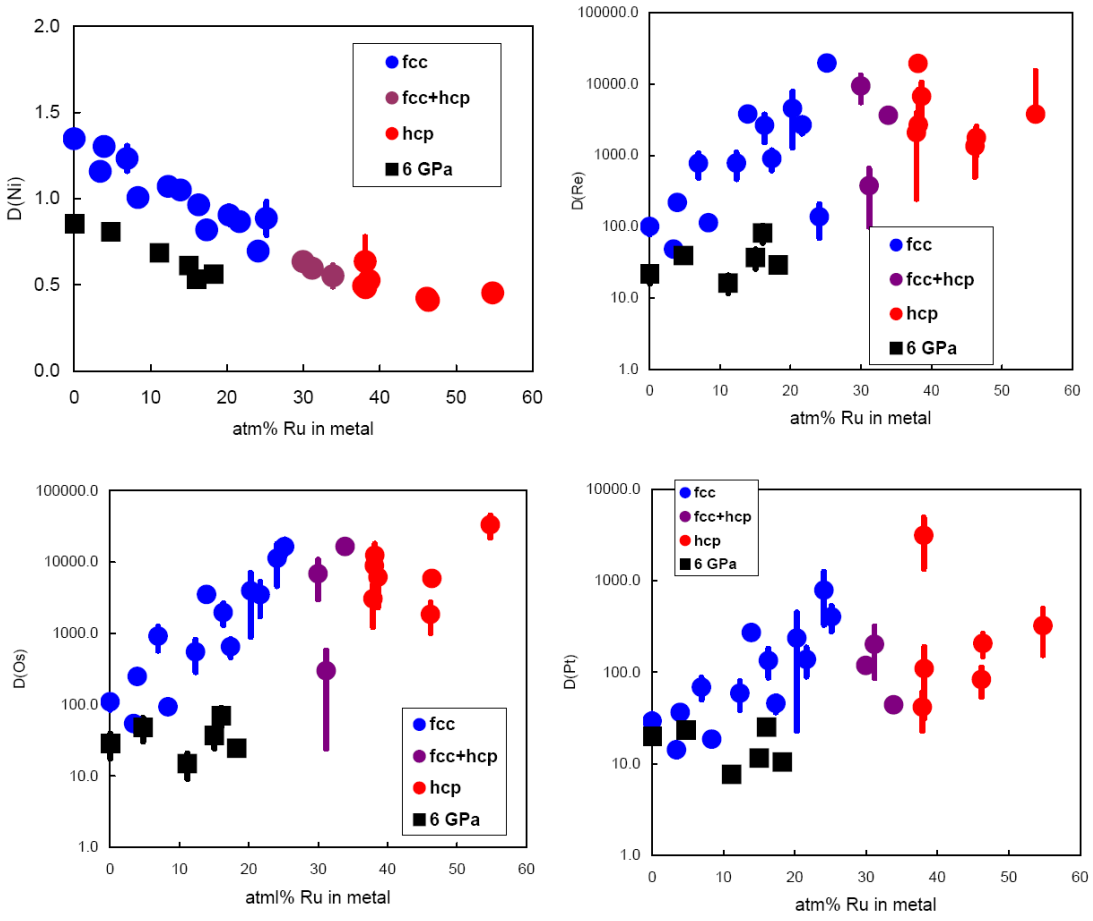

Figure 13. Graphs of the experimental D values of nickel, rhenium, osmium and platinum plotted against ruthenium content in the metal phase.

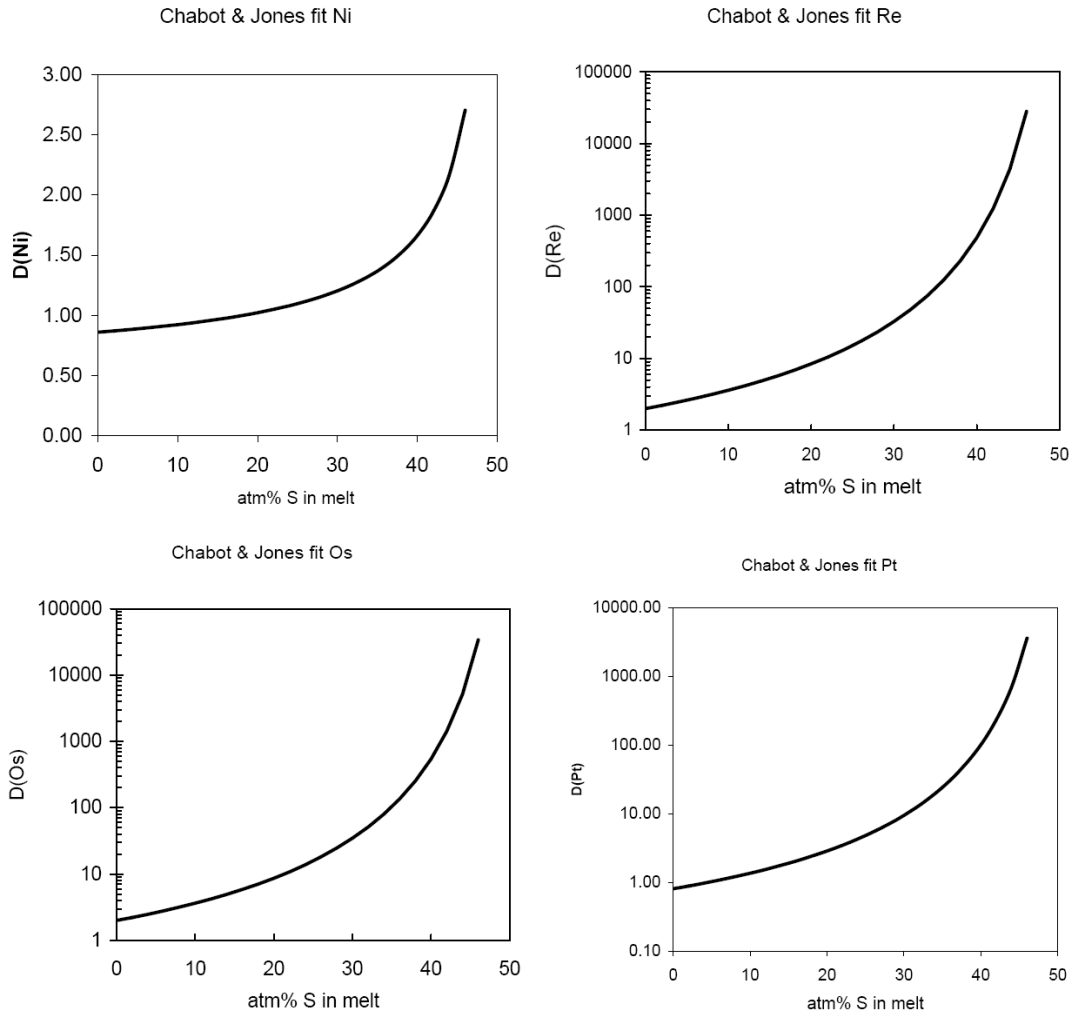

Figure 14. The Chabot and Jones parameterized D value trend plotted against atomic percent of sulfur in a melt.

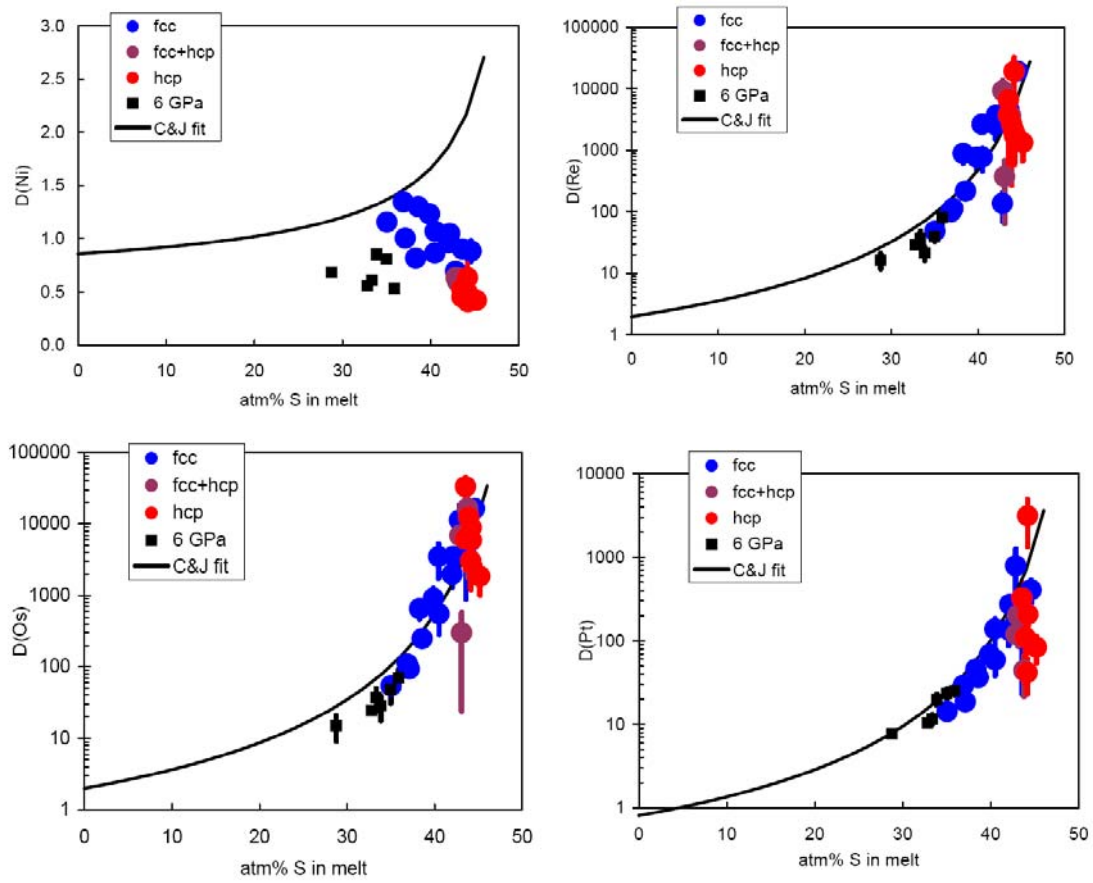

Figure 15. The experimental D values of nickel, rhenium, osmium and platinum plotted with the Chabot and Jones parameterized D value trend.

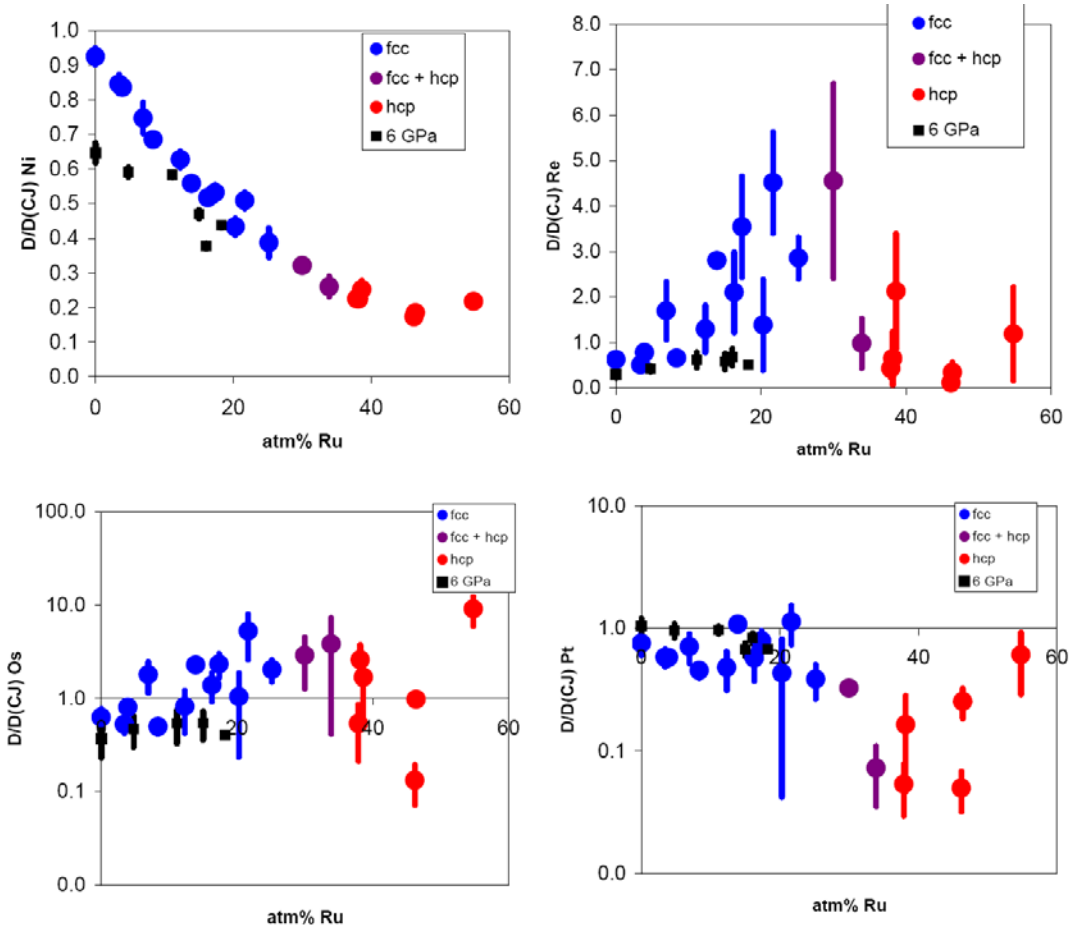

Figure 16. The normalized D values plotted against ruthenium content in the metal phase.

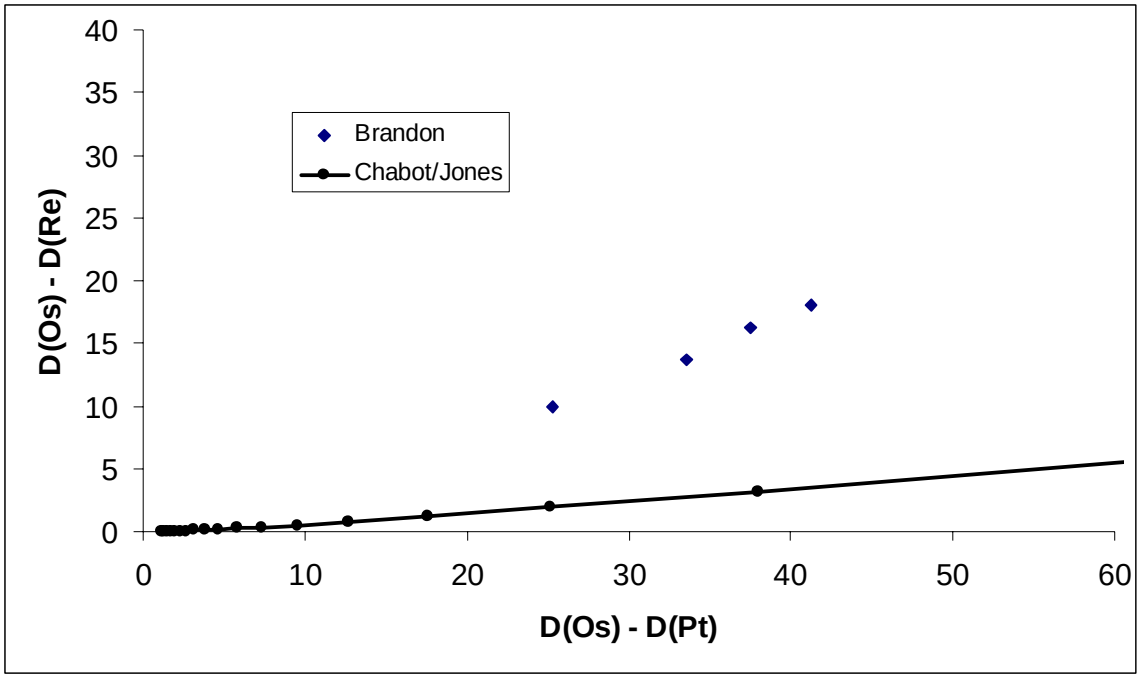

Figure 17. A plot of D_{Os}-D_{Pt} vs. D_{Os}-D_{Re} for the parameters of the core crystallization models proposed by Brandon et al. along with a plot of parameterized Chabot and Jones fcc plot of D_{Os}-D_{Pt} vs. D_{Os}-D_{Re}. Each node on the trend lines corresponds to 2 atm% sulfur.

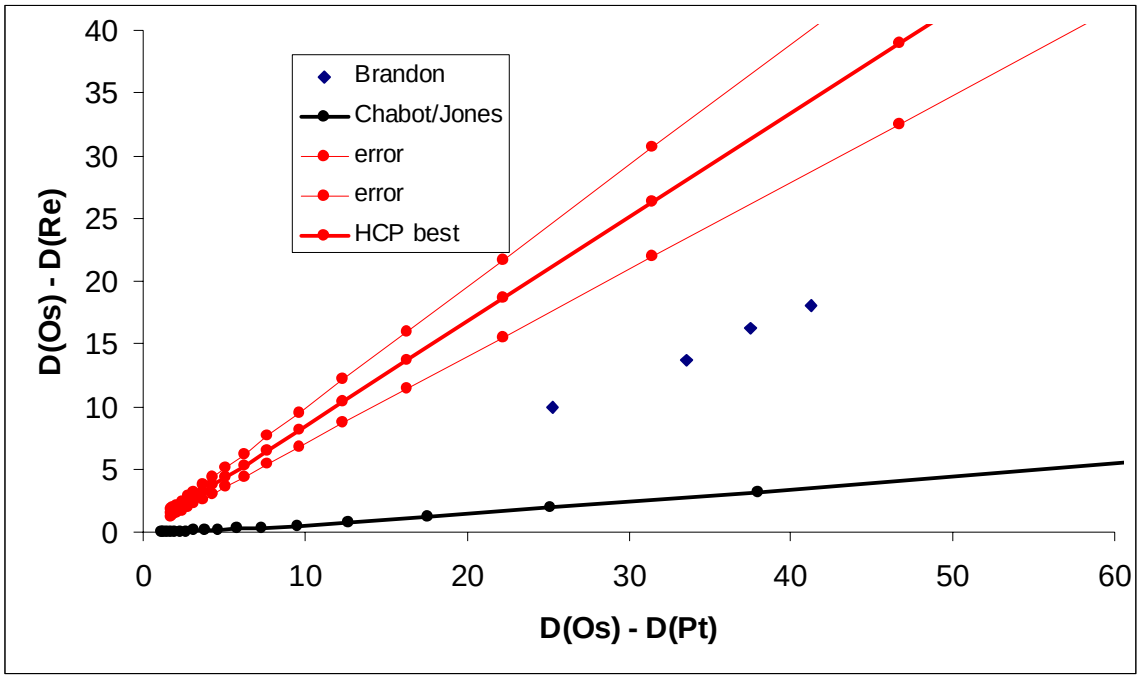

Figure 18. A graph showing the effect of the calculated fcc to hcp phase transition in the solid iron. Each node on the trend lines corresponds to 2 atm% sulfur.

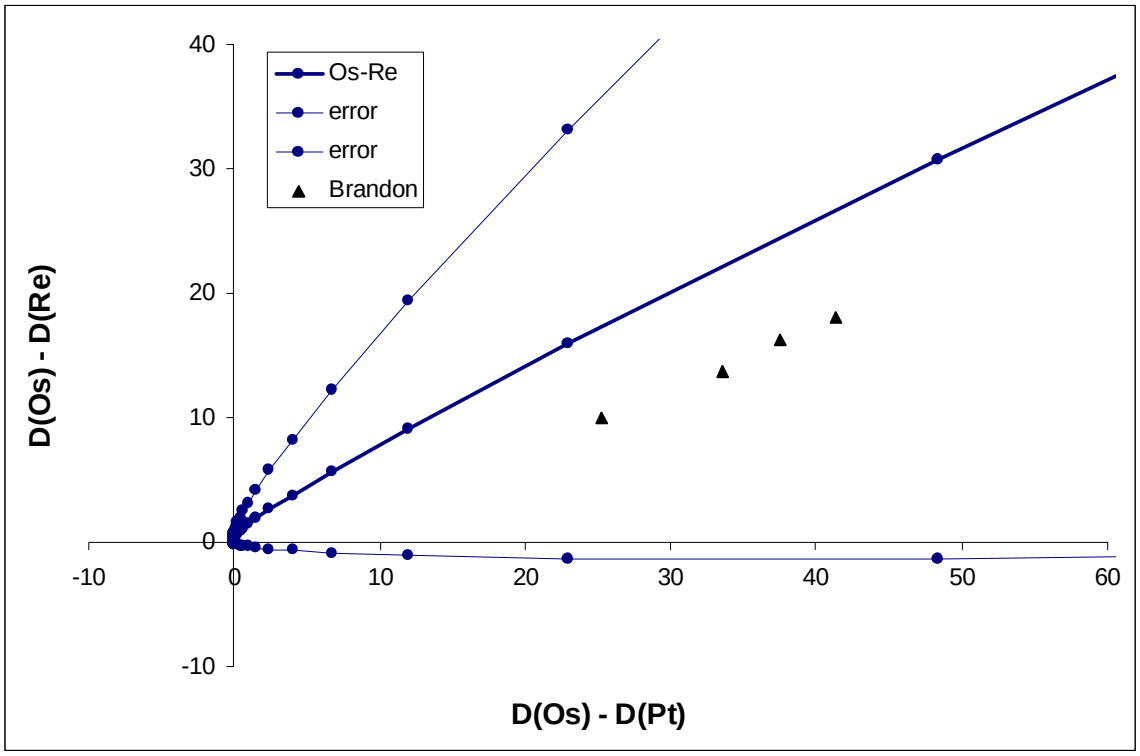

Figure 19. A graph showing the effect of the calculated 6 GPa pressure effect on the solid iron. Each node on the trend lines corresponds to 2 atm% sulfur.